1

Pulse-Laser Powered Orbital Launcher

Hiroshi Katsurayma[1], Kimiya Komurasaki[2] and Yoshihiro Arakawa[2]
[1]*Yamaguchi University*
[2]*The University of Tokyo*
Japan

1. Introduction

Some innovative plans in space development have been suspended because of high transportation costs of conventional launching systems. For example, the Japanese H2A rocket will cost $400 billion to launch a 1 GW output Solar Power Satellite (SPS) whose weight is 10^4 ton (Collins, 1993). A pulse-laser powered orbital launcher is a potential alternative to reduce those costs: a large payload ratio can be achieved because energy is provided from a ground-based laser and atmospheric air is used as a propellant.

Figure 1 shows an air-breathing pulse-laser powered vehicle ("Lightcraft") (Myrabo, 2001) with representative scales for 100 MW-class laser input. The vehicle forms plasma by focusing transmitted laser beams using a parabolic spike nozzle. The plasma absorbs the following part of the laser pulse while expanding outward. The resulting blast wave reflects on the nozzle surface and generates impulsive thrust.

Figure 2 shows a schematic view of a pulse-laser powered launching system from the ground to a Geosynchronous Earth Orbit (GEO). In the initial stage of the launch, the vehicle closes its inlet and takes air from its rear area. This flight mode is called "pulsejet mode". The inlet is opened and air is taken from the front end of the vehicle when the vehicle is accelerated sufficiently to be able to use ram-compression. This flight mode is called "ramjet mode". The inlet is again closed and on-board hydrogen is used as a propellant when the vehicle cannot obtain sufficient air at high altitudes. This flight mode is called "rocket mode." Through these three modes, the vehicle is accelerated to reach orbital velocity.

Several researchers have studied the feasibility for orbital launch using several laser propulsion systems (Toki, 1991; Kare, 1986; Humble et al., 1995; Phipps et al., 2000) , but most of them calculate flight trajectories using the thrust modeled with a fixed energy conversion efficiency. However, in an air-breathing propulsion system, the energy conversion efficiency evidently depends on its flight trajectory.

The present article introduces our realistic performance modeling in three flight modes: the performance in the pulsejet mode is modeled using measured energy conversion efficiency (Mori et al., 2004, a) and Computational Fluid Dynamics (CFD) analysis (Katsurayama et al., 2008); the performance during the ramjet mode is computed using CFD analysis (Katsurayama et al., 2003); and the performance in the rocket mode is obtained analytically with the energy conversion efficiency computed using a thermochemical equilibrium calculation (Katsurayama et al., 2003). In addition, a transfer trajectory to the GEO is proposed. The launch trajectory to its geosynchronous transfer orbit (GTO) is computed using these realistic thrust models. Finally, the feasibility of the pulse-laser

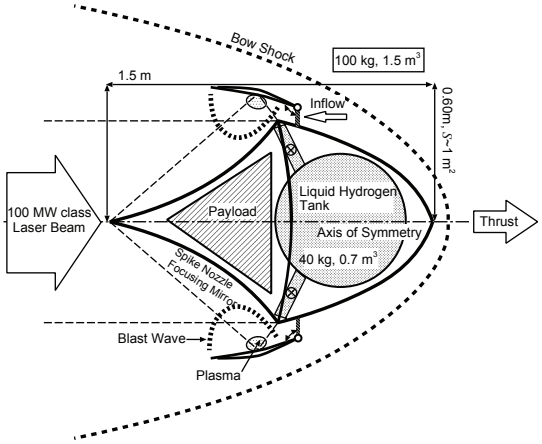

Fig. 1. Air-breathing pulse-laser powered vehicle(Myrabo, 2001).

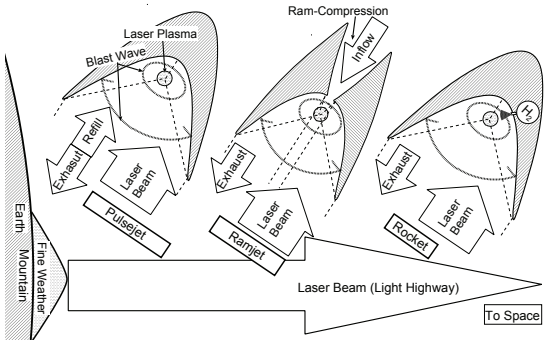

Fig. 2. A pulse-laser powered orbital launching system.

powered orbital launcher is discussed through estimation of its achievable payload mass per unit beam power and costs (Katsurayama et al., 2009).

2. Performance modeling of pulse-laser powered vehicle

2.1 Momentum coupling coefficient and blast wave energy conversion efficiency

A momentum coupling coefficient C_{m}, which is the ratio of cumulative impulse to laser energy per pulse E_{L}, is used as a performance indicator for laser propulsion. It is defined as

$$C_{\mathrm{m}} = \int_{I\ pulse} F \mathrm{d}t \Big/ E_{\mathrm{L}}, \tag{1}$$

where F denotes thrust. The laser energy absorbed in a gas is converted to the blast wave energy E_{bw}, which is the source energy necessary to drive an equivalent blast wave in a calorically perfect gas Ushio et al. (2008):

$$E_{\mathrm{bw}} = \int_{V_{\mathrm{bw}}} \left[\rho \left(e^{\mathrm{t+r}} + 1/2u^2 \right) - \rho_0 \left(e^{\mathrm{t+r}} + 1/2u^2 \right)_0 \right] \mathrm{d}V, \tag{2}$$

where V_{bw} is the volume surrounded by the blast wave, and ρ and $1/2u^2$ are the density and kinetic energy. Subscript 0 indicates the properties before laser incidence. Here, e^{t+r} is the sum of internal translational and rotational energy. On the other hand, the vibrational and electric excitation energy that are excited because of laser absorption are excluded from E_{bw} because they are newly stored in molecules and can not achieve pressure work as well as chemical potential energy. Because only E_{bw} contributes to F, C_m is proportional to the blast wave energy conversion efficiency η_{bw}

$$\eta_{bw} = E_{bw} / E_L. \tag{3}$$

Therefore, it is necessary to model the performance.

2.2 Explosion source model

According to our previous experiment (Mori et al., 2004, a;b; Mori et al., 2002) with a CO_2 TEA laser, approximately 95 % of E_L is absorbed in the form of the Laser Supported Detonation (LSD) wave (Raizer, 1977), and approximately its 45 % is converted to drive a blast wave. The remainder energy is confined in the form of chemical potential and electric excitation energy into rarefied plasma left near the focus: it is inconvertible to thrust, and is gradually lost in the form of radiation or dissipative heat flux to the surrounding. Therefore the remainder energy is excludable to reproduce this adiabatically expanding blast wave; the energy converted to the blast wave E_{bw} can be assumed to be equivalent to an instantaneous point explosion energy necessary to drive a blast wave with the same strength.

Mori et al., 2004 (a) has investigated η_{bw} by comparing measured shock speed with that calculated using a similarity solution (Kompaneets, 1960) under the assumption of ideal air. The resulting η_{bw} in the standard atmosphere was 0.43 ± 0.04, which was insensitive to E_L within the tested range of 4.0–12.8 J (Mori et al., 2004, a).

Although Wang et al. (2002) has computed the propagation of a LSD wave to investigate this energy conversion mechanism, such a computation is too expensive for our purpose to model ther thrust performance resulting from the adiabatic expansion of the blast wave whose time scale (the order of 100 μs) are much longer than that of energy absorption process (3.5 μs). In the performance modeling using our CFD analyses, the blast wave is driven by a pressurized explosion source with η_{bw}=0.43, whose radius is 1 mm and density is equal to that in the ambient atmosphere. Such an explosion source method (Steiner et al., 1998; Jiang et al., 1998; Liang et al., 2001; 2002) is familiar to simulate blast wave propagation whose time scale is much longer than that of energy input process.

Measured (Mori et al., 2004, a) and computed (Katsurayama et al., 2008) propagation of a blast wave in free space are compared to validate the blast wave reproducibility of this explosion source. Figure 3 shows the histories of the shock front radius R_{bw} and Mach number M_{bw} of the blast wave in the case of E_L=5.4 J. The CFD can reproduce the measured R_{bw} and M_{bw} after laser heating. Thereby the source model is used for computation to predict the thrust performance, and it was located at a laser focus.

2.3 Conical laser pulsejet

The thrust generation processes in a laser pulsejet with a conical nozzle were simulated to validate the performace modeling using our CFD analyses (Katsurayama et al., 2008). Figure 4 schematically shows sequential thrust generation processes in the laser pulsejet with a simple conical nozzle of its half apex angle α. In an energy absorption process (a), plasma is produced near the laser focus. The plasma absorbs laser energy in the form of a LSD wave. The large

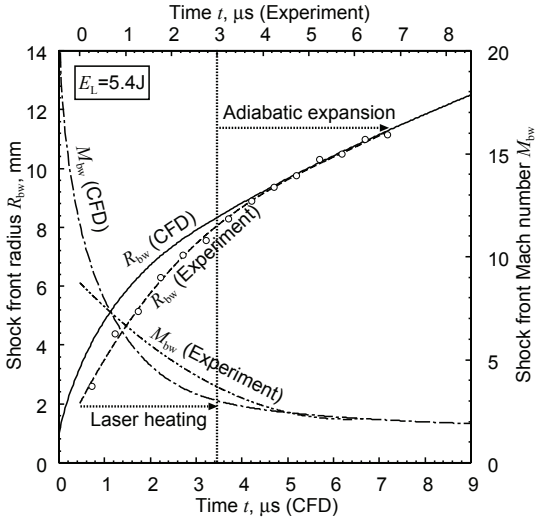

Fig. 3. Comparison of the CFD and the experiment on R_{bw} and M_{bw} in the explosion in free space. (CFD: η_{bw}=0.43; Experiment (Mori et al., 2004, a) : η_{bw}=0.43±0.04)

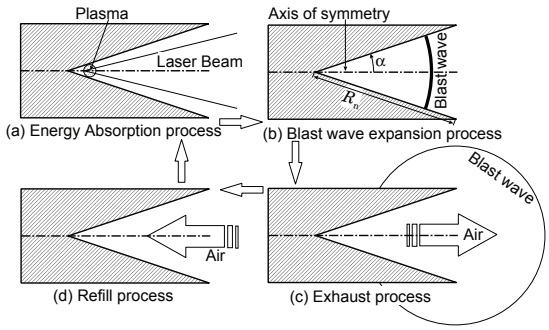

Fig. 4. Schematic of a laser pulsejet engine cycle.

part of the absorbed energy is used to drive a high-pressure blast wave in the surrounding air. In a blast wave expansion process (b), the blast wave imparts an impulsive thrust directly to a nozzle wall; thereby, main thrust is produced. In exhaust (c) and refill (d) processes, the air in the nozzle is exhausted and fresh air is taken in. Additional thrust will be produced in these processes.

Because the exhaust-refill prcoesses results from an adiabatically expanding blast wave after laser heating, an explosion source is used to drive the blast wave instead of solving a laser abosrption process. Figures 5 and 6 respectively show the thrust history and corresponding pressure contours of a conical laser pulsejet. Δp in the captions of pressure contours shows the interval of the contours. An explosion starts at t=0 (see Fig. 6(a)). A shock wave reaches the nozzle exit at t_0 μs as shown in Fig. 6(b). F_0 is the thrust at t=t_0. After t=t_0, the heated air starts to be exhausted and thrust decreases gradually. At t=t_1 (see Fig. 6(c)), thrust becomes zero. Thrust becomes negative because of the rarefaction wave behind the shock wave and

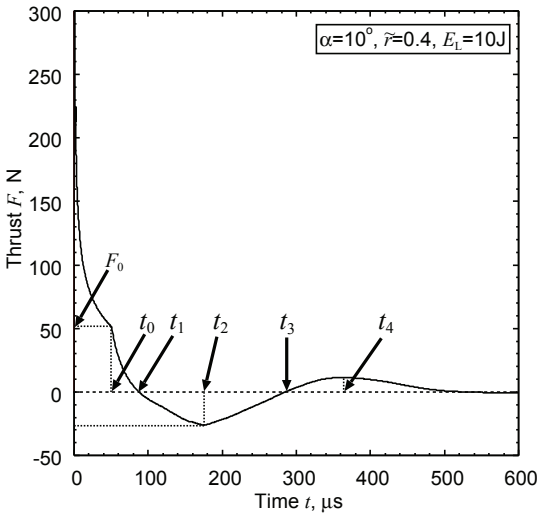

Fig. 5. Thrust history. (η_{bw}=0.43)

thrust takes a minimum value at $t=t_2$. The gauge pressure becomes negative for the entire region inside of the nozzle, as seen in Fig. 6(d). At $t=t_3$ (see Fig. 6(e)), thrust reverts to zero; subsequently, thrust has a second peak at $t=t_4$. After $t=t_4$, thrust oscillates and the oscillation attenuates gradually.

Figure 7 shows measured (Mori et al., 2004, b) and computed relationships between C_m and α. The computation reproduces the C_m decreasing tendency. The processes until the shock front of a blast wave reaches the nozzle exit are similar regardless of the nozzle apex angle. However, after the blast wave leaves the nozzle edge, the behavior of the rarefaction wave induced behind the shock wave depends greatly on the nozzle apex angle. In the case of small apex angles, succsessive refilling mechanisms with vortices are activated by the prominently evolved rarefaction wave, in contrast, in the case of large apex angles, this mechanims do not appear due to the moderate evolution of the rarefaction wave. This difference was found to result in the decreasing tendency of the momentum coupling coefficient. More detailed descriptions of these phenomena is found in Katsurayama et al. (2008).

Because the computed C_m is in good agreement with measured data in the cases of small α, our CFD analyses have the capability for predicting the thrust performace of a pulse-laser powerd launcher. Although the deviation from the measurement increases with increasing α, this unpredictability is insignificant because the cause is attributable to the not-optimized geomertical relation between the LSD propagation distance and nozzle length (Katsurayama et al., 2008).

2.4 Laser ramjet

C_m during the laser ramjet mode was computed in our previous CFD analyses (Katsurayama et al., 2003). A blast wave is again driven by an explosion source model with η_{bw} which depends on atmospheric pressure (Katsurayama et al., 2009).

Figure 8 shows a part of computational results, and these results (Katsurayama et al., 2003) have showen that C_m in the ramjet mode is insensitive to laser energy E_L and depends only on flight conditions. Therefore, the performance is obtained from the map of C_m, which is

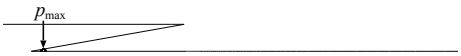

(a) t=0 μs
(p_{max}=3.77×10^3 atm, p_{min}=1.00 atm, Δp=1.26×10^2 atm)

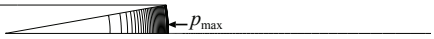

(b) t=50 $\mu s \cong t_0$
(p_{max}=3.99 atm, p_{min}=1.00 atm, Δp=9.98×10^{-2} atm)

(c) t=88 $\mu s \cong t_1$
(p_{max}=2.27 atm, p_{min}=4.32×10^{-1} atm, Δp=6.14×10^{-2} atm)

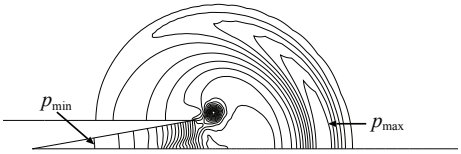

(d) t=176 $\mu s \cong t_2$
(p_{max}=1.18 atm, p_{min}=3.70×10^{-1} atm, Δp=2.70×10^{-2} atm)

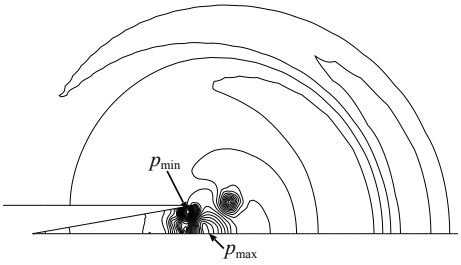

(e) t=284 $\mu s \cong t_3$
(p_{max}=1.18 atm, p_{min}=4.79×10^{-1} atm, Δp=2.34×10^{-2} atm)

Fig. 6. Typical pressure contours of the conical laser pulsejet.

constructed using CFD analyses under the conditions of 16 pairs of atmospheric density ρ_∞ and flight Mach number M_∞. The map of C_m is shown in Fig. 9 with the fitting function of M_∞ and ρ_∞

$$C_m(M_\infty,\rho_\infty) = \left[0.04M_\infty^2 - 1.81M_\infty + 19.00\right] \times \left[0.35\left(\log_{10}\rho_\infty\right)^2 + 5.01\left(\log_{10}\rho_\infty\right) + 13.06\right], \quad (4)$$

which is used to calculate the flight trajectory. The value of C_m decreases with decreasing ρ_∞ because of the decrease in a captured mass flow rate. It also decreases with increasing M_∞ because the blast wave quickly leaves the nozzle because of the increase in the engine flow speed.

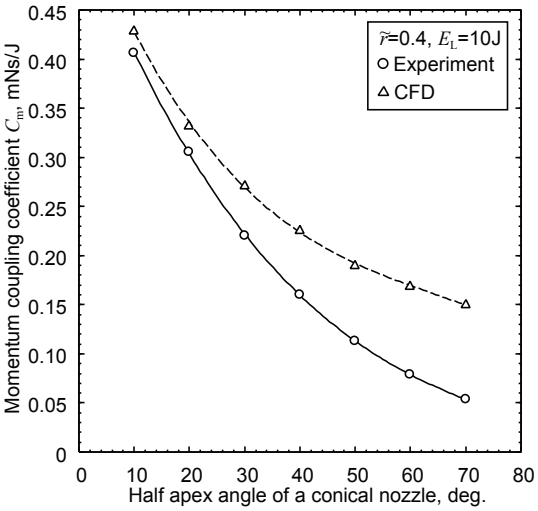

Fig. 7. Relationship between C_m and α. (CFD: η_{bw}=0.43; Experiment: η_{bw}=0.43±0.04)

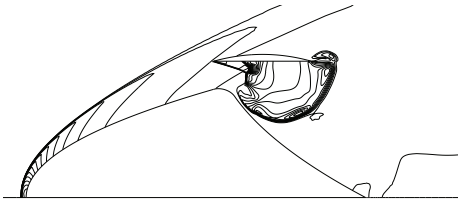

(a) At t=12 μs. (p_{max}=2.27 atm, p_{min}=2.1×10^{-2} atm, Δp=0.11 atm)

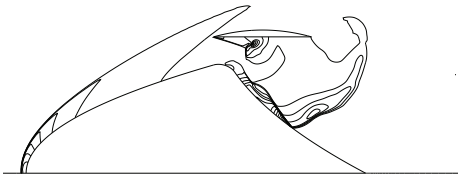

(b) At t = 20 μs. (p_{max}=4.63atm, p_{min}=2.1×10^{-2} atm, Δp=0.23 atm)

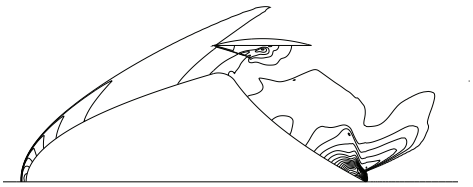

(c) At t = 38 μs. (p_{max}=4.27 atm, p_{min}=2.0×10^{-2} atm, Δp=0.21 atm)

Fig. 8. Typical pressure contours of the laser ramjet: E_L=400 J, H=20 km and M_∞=5.

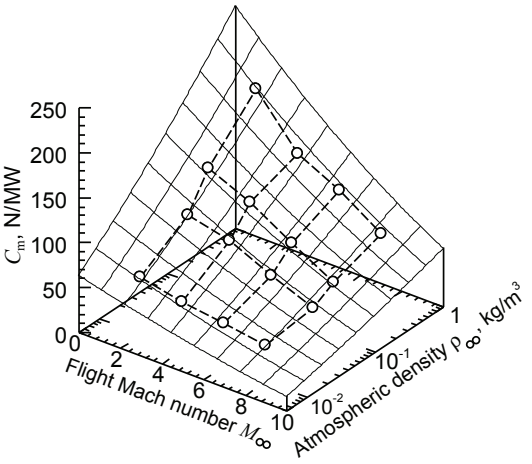

Fig. 9. C_m map of the laser ramjet.

2.5 Laser rocket

Because the vehicle flies in a near-vacuum environment in the rocket mode, its thrust depends only on the nozzle expansion ratio. The self-similar solution in a conical nozzle (Simons et al., 1977) is available to estimate C_m. Assume that the blast wave propagates in the hydrogen propellant expanding to a vacuum. In such a case, C_m is modeled as

$$C_m = \sqrt{2\dot{m}_p \eta_{bw,rocket}/P_L}\sin^2\alpha \Big/ \left[2\pi\left(1-\cos\alpha\right)\right], \tag{5}$$

where $\dot{m}_p$ and P_L respectively represent the mass flow rate of hydrogen propellant and time-averaged laser power. The apex angle of the nozzle cone α is set to 30°which is almost equivalent to the value of the Lightcraft used in the CFD analysis of the ramjet mode.
The value of η_{bw} in the rocket mode is calculated analytically by solving the propagation of a LSD in hydrogen propellant using our previous numerical model (Katsurayama et al., 2003) obtained by combining a plain Chapman-Jouguet detonation relation and chemical equilibrium calculation, resulting in $\eta_{bw,rocket} = 23.5\%$.

3. Feasibility of pulse-laser orbital launcher

3.1 Light highway

The pulse-laser powered orbital launcher requires a laser base with average output of 100 MW$\sim$1 GW. For development of such a high-powered laser base, the cost of a laser transmitter is expected to predominate over the costs required for other systems such as cooling and power supply (Kare, 2004). Thereby, the cost-reduction of the laser transmitter is indispensable for the launching system. An optical phased array with diode lasers (Kare, 2004; Komurasaki et al., 2005) will reduce the cost because existing laser technology is applicable and mass-production effect is expectable. Moreover, launch using only a laser base is realistic. Furthermore, several obstacles on beam transmission should be assessed briefly to discuss the launching system feasibility. If the beam is a Gaussian beam whose respective aperture and wavelength are 1 m and 1 μm, the total spreading angle is 1.2×10^{-6} rad. The energy loss caused by beam diffraction is acceptable because the beam radius spreads to only 1.19 m at the

transmission distance of 500 km, which is the typical value required for the launching system. The beam spread, attenuation, and refraction caused by nonlinear effects of the atmosphere, such as the variation of atmospheric refraction index, thermal blooming, Rayleigh, Raman and Mie scattering, have been analyzed for the ORION project (Phipps et al., 1996; Cambell, 1996), which is intended to remove debris on orbits using a pulse laser. Nonlinear effects are inferred to be negligible for transmission with a beam power density under a threshold determined by a laser pulse width and wavelength.

To avoid the whipping phenomenon of the beam center caused by atmospheric turbulence, the launch site should be built on the top of a mountain where the weather is expected to always be fine and for which scintillation caused by atmosphere is small. A location where an astronomical observatory has been built is suitable if a vehicle is launched at a time without clouds or turbulence. For example, Mauna Kea in Hawaii has no cloud cover for 90% of the days in a year.

In addition, an ongoing study (Libeau et al., 2002) proposes a vehicle shape with which the vehicle can maintain its center axis parallel to the beam direction by generating thrust vector and torque automatically in the direction that allows it to retain aerodynamic stability. Both directions of the flight and beam can be maintained as vertical to the ground using this technology. Therefore, vehicle tracking and beam pointing are unnecessary for the launching system. The vehicle can be transferred to space along a "light highway" (Myrabo, 2001) constructed vertically from the ground, as shown in Fig. 2.

3.2 Proposed trajectory to GEO

Considering requirements for beam transmission, the vehicle is accelerated vertically in a short distance along the light highway. Figure 10 shows a trajectory to a GEO through the pulse-laser powered launcher and an upper-stage propulsion system for the Hohmann transfer. The vehicle is launched from the equator through the pulse-laser powered launcher; it is accelerated rapidly to Δv_{L}. The vehicle then reaches an apogee point beyond the GEO through inertial flight to use the Δv_{L} efficiently. The structure weight of laser propulsion is detached at the apogee point, and the upper-stage propulsion system is burned. The detached structure is attracted to the earth and it is incinerated during reentry into the atmosphere.

Figure 11 shows the variation of Δv_{L} and the velocity increment Δv_{H} required for the Hohmann transfer with cut-off velocity v_{c}, which is the flight velocity when laser propulsion is terminated. The required Δv_{L} and Δv_{H} are 18.85 and 1.84 km/s, respectively, if v_{c}=10.6 km/s is chosen.

Electric propulsion is available for the upper-stage propulsion system by virtue of an abundant electricity supply from the cells if solar cells are transferred to construct an SPS. Using the Hall thruster, whose specific impulse $I_{\mathrm{sp,EP}}$ is 2000 s, the transfer to the GEO takes a spiral trajectory. As a result of calculating them by solving equations of motion (Spencer et al., 1995; Kluever et al., 1998) without trajectory optimization, the effective velocity increment $\Delta v_{\mathrm{spiral}}$ (Spencer et al., 1995) through the upper-stage propulsion is estimated as 3.68 km/s. The resulting payload ratio λ_{u} of the upper stage is

$$\lambda_{\mathrm{u}} = 1 - \int_{\mathrm{spiral}} \frac{2\eta_{\mathrm{EP}} \left(P_{\mathrm{EP}} / m_{\mathrm{u},0} \right)}{\left(g I_{\mathrm{sp,EP}} \right)^2} \mathrm{d}t \Bigg/ \left(1 - \varepsilon_{\mathrm{EP}} \right) = 0.83. \tag{6}$$

where the propulsion system efficiency η_{EP} and the structure weight coefficient $\varepsilon_{\mathrm{EP}}$ are assumed respectively as 65% (Kluever et al., 1998) and 0.1. The ratio of power to the initial

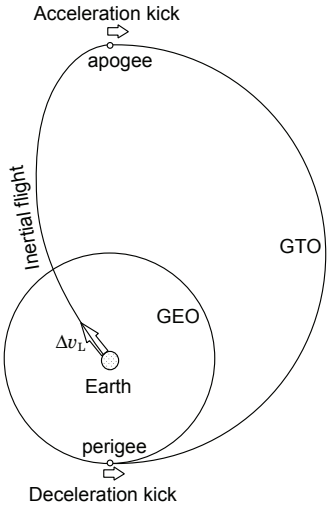

Fig. 10. Proposed trajectory to GEO.

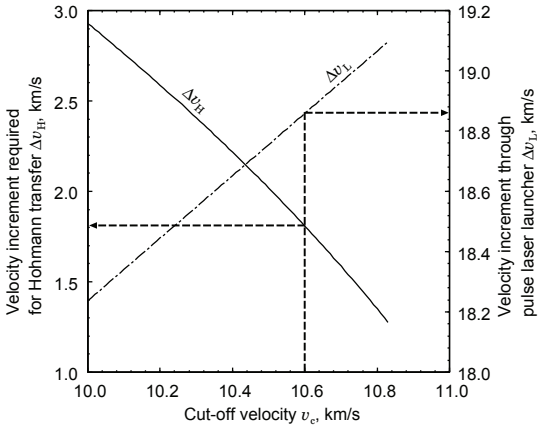

Fig. 11. Variation of the velocity increment through the pulse-laser powered launcher and the velocity increment required for the Hohmann transfer with cut-off velocity.

upper-stage weight $(P_{EP}/m_{u,0})$ is set to 100 W/kg in view of the ratio of power to weight of the 1 GW-output SPS.
v_c=10.6 km/s and λ_u=0.83 are used in the calculation of launch trajectories described in § 3.4.

3.3 Mode switching criteria

The pulsejet mode should be switched to the ramjet mode when the blast wave becomes free from propagation over the inlet because of the vehicle acceleration. However, numerous CFD analyses are necessary to model the timing correctly because it depends on E_L and flight conditions. The present model therefore chooses the safest timing: the mode is switched when the flow in the vehicle is free from choking by laser heating. An engine cycle, as shown

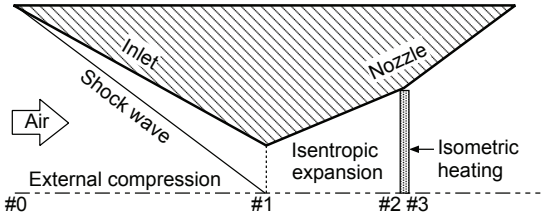

Fig. 12. Engine cycle for assessing heat-choking.

in Fig. 12, is analyzed to assess heat-choking. In this cycle, the air is taken in at location #0 through an effective inlet area

$$A_0 = S_{\mathrm{v}} \times \mathrm{C.A.R.}, \tag{7}$$

where S_{v} and C.A.R. are the maximum cross sections of the vehicle and the capture area ratio. The captured air is compressed externally from #0 to #1 as

$$u_1 = \eta_{\mathrm{d}} u_0 \tag{8}$$

where u and η_{d} are the flow velocity of the air and diffuser efficiency. η_{d} and C.A.R. are obtained using CFD analysis on the Lightcraft. With increasing M_∞, η_{d} decreases from 0.72 to 0.62 and C.A.R increases from 0.31 to 0.71 (Katsurayama et al., 2004). The air is then expanded isentropically from #1 to #2 to delay heat-choking at #3. Finally, it is laser-heated isometrically from #2 to #3. The Mach number at #3 is calculated as

$$M_3 = u_3 \Big/ \sqrt{\gamma R T_3} = u_2 \Big/ \sqrt{\gamma R \left[T_2 + \eta_{\mathrm{bw}} \eta_{\mathrm{trans}} P_{\mathrm{L}} / \left(C_{\mathrm{p}} \dot{m}_{\mathrm{air}} \right) \right]}$$

Herein, T and $\dot{m}_{\mathrm{air}}$ is temperature and the captured mass flow rate. Respectively, R, C_{p} and γ denote the gas constant, the constant pressure specific heat, and the specific heat ratio of ideal air. Furthermore, η_{trans} is the transmission efficiency of the laser beam. The pulsejet mode is switched to the ramjet mode when

$$M_3 = 1. \tag{9}$$

In the ramjet mode, the mass flow rate taken from the inlet decreases with altitude because of the decrease in the atmospheric density. Finally, the acceleration of the vehicle becomes zero because of the balance between thrust and aerodynamic drag, at the time when the flight mode is switched to the rocket mode.

3.4 Computed launch trajectory and payload ratio

A launch trajectory to the GEO is calculated by solving the following equation of motion by the 4th order Runge-Kutta scheme.

$$m_{\mathrm{v}} \frac{\mathrm{d}v}{\mathrm{d}t} = \overline{F} - \frac{1}{2} \rho_\infty v^2 S_{\mathrm{v}} C_{\mathrm{d}} - m_{\mathrm{v}} g_0 \left[R_{\mathrm{E}} / \left(R_{\mathrm{E}} + h \right) \right]^2 \tag{10}$$

Therein, S_{v}, v and m_{v} are the maximum cross sections of the vehicle, the flight velocity, and the vehicle weight. Also, g_0, R_{E} and h respectively indicate the gravity acceleration on the ground, the radius of the earth and the flight altitude. An aerodynamic drag coefficient C_{d} is obtained using the CFD analysis on the Lightcraft; it varies from 0.15 to 0.64 depending

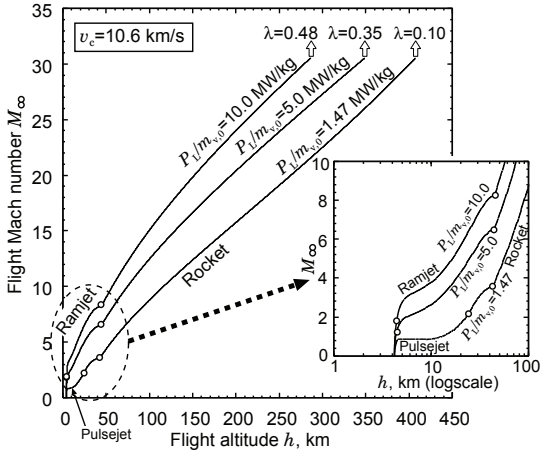

Fig. 13. Flight Mach number vs. flight altitude.

on M_∞ (Katsurayama et al., 2004). Flight conditions are determined by tracing the trajectory. Time-averaged thrust $\overline{F}$ in each mode is estimated using C_m modeled in § 2 as

$$\overline{F} = C_m \eta_{trans} P_L. \tag{11}$$

Herein, if the laser transmitter is the phased array with an effective broad aperture, the fraction of beamed energy contained in a main-lobe of beam is theoretically predictable. It is independent of the transmission distance; η_{trans} is set to its predicted value of 72 % (Komurasaki et al., 2005) on the assumption that the nonlinear effects attributable to the atmosphere negligibly affect the beam transmission.

As the result of the trajectory calculation, the payload ratio λ is estimated as

$$\lambda = \left\{ 1 - \int_{\text{Rocket mode}} \dot{m}_p dt \Big/ \left[m_{v,0} (1 - \varepsilon_L) \right] \right\} \lambda_u, \tag{12}$$

where $m_{v,0}$ is an initial vehicle mass and the upper stage payload ratio λ_u=0.83 is used (Katsurayama et al., 2009). The structure weight coefficient of the pulse-laser powered vehicle ε_L is set to 0.1 in view of the simple structure of the vehicle.

The vehicle is launched at h=4200 m equal to the altitude of Mauna Kea. The calculation is terminated when the vehicle is accelerated to the cut-off velocity (Katsurayama et al., 2009) v_c=10.6 km/s. Figure 13 shows the trajectories and λ for several specific beam power $P_L/m_{v,0}$. The ramjet period and λ decrease with decreasing $P_L/m_{v,0}$. The ramjet mode becomes unavailable at $P_L/m_{v,0}$<1.47 MW/kg. The beam transmission requests the longest distance of 400 km and the longest duration of 160 s.

Figure 14 shows the variations of the payload mass per 1 MW beam power m_{pl}/P_L and λ with $P_L/m_{v,0}$. Although λ increases with $P_L/m_{v,0}$, m_{pl}/P_L has the maximum 0.084 kg/MW at $P_L/m_{v,0}$ =2.42 MW/kg. Therefore, this

$$(P_L/m_{v,0})_{opt} = 2.42 \tag{13}$$

is the optimum condition of minimizing the building cost of a laser transmitter.

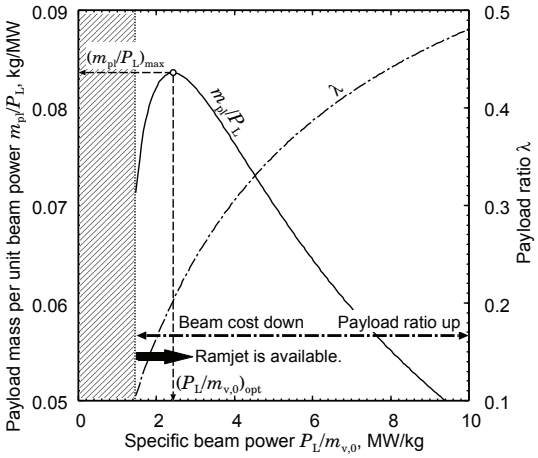

Fig. 14. Variation of payload mass per unit beam power and payload ratio with specific beam power.

C_{LT}, \$/W	C_E, \$/kWh	C_{VP}, % \$/kg	η_{DL}, %
10	0.06	1,000	40

Table 1. Costs and efficiency considered in cost estimation.

3.5 Launch cost

This section estimates the cost of the mission in which a 10^4-ton SPS is transferred to a GEO through many pulse-laser powered orbital launches. Although the cost estimation of a laser transmitter with 100 MW∼1 GW-output is difficult, the most promising technology for high power output is to coherently couple lasers such as solid, fiber, and diode lasers (Shirakawa et al., 2002; Sanders et al., 1994). The cost of the laser transmitter can be estimated as shown in Table 1 if the coherent coupling is applicable to the array of diode lasers whose production cost per unit of power is currently the cheapest. The cost of the laser transmitter C_{LT} is assumed to be a current diode laser price per unit output power (Kare, 2004). Other costs, such as that for the cooling system, power supply and maintenance, are not considered because they are negligibly small compared with C_{LT} (Kare, 2004). The general electricity cost in Japan is C_E. The vehicle production cost C_{VP} is the cost per unit vehicle weight estimated for the Lightcraft whose dry mass and diameter are 100 kg and 1.4 m (Richard et al., 1988). η_{DL} is the energy conversion efficiency of a general diode laser (Kare, 2004). To compare costs of the pulse-laser powered launcher and an existing commercial launcher, the launch cost is defined in the form of redeeming the cost of the laser transmitter.

$$\frac{\text{Launch cost}}{\text{Payload mass}} = \frac{\left[C_{LT}/n_L + (C_E/\eta_{DL})\,t_{flight}\right]P_L + C_{VP}m_{v,0}}{m_{pl}} = \frac{C_{LT}/n_L}{\left(m_{pl}/P_L\right)_{max}} + \frac{(C_E/\eta_{DL})\,t_{flight}}{\left(m_{pl}/P_L\right)_{max}} + \frac{C_{VP}}{\lambda} \quad (14)$$

For that calculation, a payload is divided and transferred through n_L launchings. Furthermore, $\left(m_{pl}/P_L\right)_{max}$ (=0.084) is used on the basis of using $(P_L/m_{v,0})_{opt}$, on the condition of which

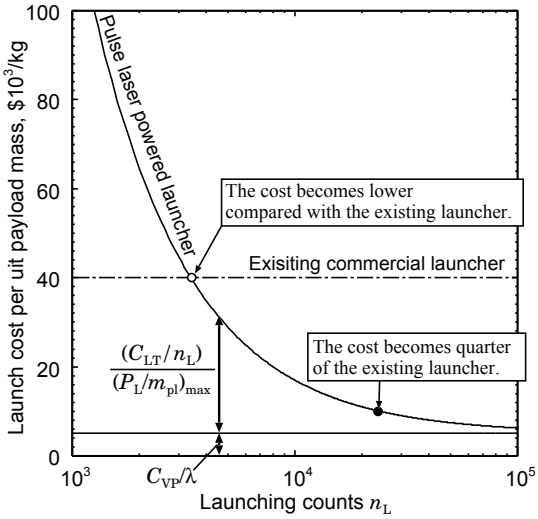

Fig. 15. Variation of launch cost per unit payload mass with n_L.

the resulting λ and flight time t_{flight} are 0.20 and 112 s. The first term in the second line of Eq. (14) is the redemption of the laser transmitter. The second and third terms correspond to the electricity and vehicle production cost. Labor costs are omitted because a generally published launch cost, e.g. $80 million per launch of the Japanese H2A rocket, includes only the rocket's production cost.

Figure 15 shows the variations of the launch cost per unit payload mass with n_L of the pulse-laser powered orbital launcher and an existing commercial launcher. The cost of the existing launcher is assumed to be $80 million per launch. The cost of the laser transmitter is predominant when n_L is less than 10^3. On the other hand, the electricity cost is negligible. The launch cost decreases with increasing n_L and the cost of the laser transmitter is recovered at 3,500 launches compared with the existing launcher. The cost becomes a quarter of the existing launcher at n_L=24,000. When n_L is greater than 10^5, the cost of the laser transmitter is completely recovered and the cost comprises only the vehicle production cost of approximately $5,000 per unit of payload mass. The electricity cost remains negligibly small over n_L=10^5.

Consequently, if the laser base of 5 GW-class output is available, the launcher has the capability of approximately 0.5 ton payload/launch. It is expected to deliver the 10^4 ton SPS through 24,000 launches at a quarter of the cost of an existing launcher. Moreover, if the mass-production effect can reduce C_{VP} to $100/kg, the launcher will cost about a tenth of the current mode.

4. Summary

Orbital launching from the ground to a GEO using the pulse-laser powered launcher is calculated using the performance modeled in the pulsejet, ramjet and rocket modes. Consequently, it can transfer 0.084 kg payload per 1 MW beam power to the GEO. The cost becomes a quarter of that of existing systems if one can divide a single launch into 24,000

multiple launches. Furthermore, if the payload is transferred through 10^5 launches, the launching system can reduce the cost to the order of $\$10^3$ per unit of payload mass.

5. References

Campbell, J. W. (1996). Project ORION: Orbital Debris Removal Using Ground-Based Sensors and Lasers, NASA TM-108522

Collins, P. (1993). The Promise of Electricity from Space for World Economic Development, *Proceedings of 5th International Energy Conference*, Vol. 3, pp. 50-59.

Humble, W. E. and Pierson, B. L. (1995). Maximum-Payload Trajectories for a Laser-Propelled Launch Vehicle, *Journal of Guidance, Control and Dynamics*, Vol. 18, No. 6, pp.1259–1266.

Jiang, Z., Takayama, K., Moosad, K. P. B., Onodera, O., and Sun, M. (1998). Numerical and Experimental Study of a micro-blast wave generated by pulsed-laser beam focusing, *Shock Waves*, Vol. 8, No. 6, pp.337-349.

Kare, J. T. (1986). Trajectory Simulation for Laser Launching, *Proceedings of the 1986 SDIO/DARPA Workshop on Laser Propulsion*, Vol. 2, pp.61-77.

Kare, T. J. (2004). Modular Laser Optics for HX Laser Launch, *Proceedings of the 3rd International Symposium on Beamed Energy Propulsion*, AIP Conference Proceedings, Vol.766, pp. 128-139.

Katsurayama, H., Komurasaki, K., Momozawa, A., and Arakawa, Y. (2003). Numerical and Engine Cycle Analyses of a Pulse Laser Ramjet Vehicle, *Transactions of the Japan Society for Aeronautical and Space Sciences, Space Technology Japan*, Vol. 1, pp. 9-16.

Katsurayama, H., Ushio, M., Komurasaki, K., and Arakawa, Y. (2004). Analytical Study on Flight Performance of a RP Laser Launcher, *Proceedings of 3rd International Symposium on Beamed Energy Propulsion*, AIP Conference Proceedings, Vol. 766, pp.117-127.

Katsurayama, H., Komurasaki, K., Hirooka, Y., Mori, K. and Arakawa, Y. (2008). Numerical Analyses of Exhaust and Refill Processes of a Laser Pulsejet, *Journal of Propulsion and Power*, Vol. 24, No. 5, pp.999-1006.

Katsurayama, H., Komurasaki, K., and Arakawa, Y. (2009). A Preliminary Study of Pulse-Laser Powered Orbital Launcher, *ACTA Astronautica*, Vol. 65, No. 7-8, pp.1032-1041.

Kompaneets, A. S. (1960). A point explosion in an inhomogeneous atmosphere, *Soviet Physics Doklady*, Vol. 5, No. 1, pp.46-48.

Komurasaki, K., Nakagawa, T., Ohmura, S., and Arakawa, Y. (2005). Energy Transmission in Space Using an Optical Phased Array, *Transactions of the Japan Society for Aeronautical and Space Sciences Space Technology Japan*, Vol. 3, pp. 7-11.

Liang, S.-M., Hsu, J.-L.,, and Wang, J.-S. (2001). Numerical Study of Cylindrical Blast-Wave Propagation and Reflection, generated by pulsed-laser beam focusing, *AIAA Journal*, Vol. 39, No. 6, pp.1152-1158.

Liang, S.-M., Wang, J.-S., and Chen, H. (2002). Numerical Study of Spherical Blast-Wave Propagation and Reflection, generated by pulsed-laser beam focusing," *Shock waves*, Vol. 12, No. 1, pp.59-68.

Libeau, M. A. and Myrabo, L. N. (2002). Combined Theoretical and Experimental Flight Dynamics Investigation of a Laser-Propelled Vehicle, AIAA Paper 2002-3781.

Mori, K., Komurasaki, K., and Arakawa, Y. (2002). Influence of the Focusing f Number on Heating Regime Transition in Laser Absorption Waves, *Journal of Applied Physics*, Vol.92, No.10, pp.5663-5667.

Mori, K., Komurasaki, K., and Arakawa, Y. (2004). Energy Transfer from a Laser Pulse to a Blast Wave in Reduced-Pressure Air Atmospheres, *Journal of Applied Physics*, Vol. 95, No. 11, pp. 5979-5983.

Mori, K., Komurasaki, K., and Arakawa, Y. (2004). Nozzle Scale Optimum for the Impulse Generation in a Laser Pulsejet, *Journal of Spacecraft and Rockets*, Vol. 41, No. 5, pp. 887-889.

Myrabo, L. N. (2001). World Record Flights of Beam-Riding Rocket Lightcraft: Demonstration of "Disruptive" Propulsion Technology, AIAA Paper 2001-3798.

Phipps, C. R., Reilly, P. R., and Campbell, J. W. (2000). Optimum Parameters for Laser Launching Objects into Low Earth Orbit, *Laser and Particle Beams*, Vol. 18, pp.661-695.

Phipps, C. R., Friedman, H., Gavel, D., Murray, J., Albrecht, G., George, E. V., Ho, C., Priedhorsky, W., Michaelis, M. M., and Reilly, J. P. (1996). ORION: Clearing Near-Earth Space Debris Using a 20-kW, 530-nm, Earth-Based, Repetitively Pulsed Laser, *Laser Particle Beams*, Vol. 14, pp. 1-4.

Steiner, H., Gretler, W., and Hirschler, T. (1998). Numerical Solution for Spherical Laser-Driven Shock Waves, *Shock Waves*, Vol. 8, No. 3, pp.139-147.

Toki, K. (1991). Conceptual Study of Laser Direct Launch, *The Journal of Space Technology and Science*, Vol. 8, No. 2, 1991, pp. 23-31.

Wang, T.-S., Chen, Y.-S., Liu, J., Myrabo, L. N., and Mead, F. B. Jr. (2002). Advanced Performance Modeling of Experimental Laser Lightcraft, *Journal of Propulsion and Power*, Vol. 18, No. 6, pp. 1129-1138.

Spencer, D. B. and Robert, D. C. (1995). Designing Continuous-Thrust Low-Earth-Orbit to Geosynchronous-Earth-Orbit Transfers, *Journal of Spacecraft and Rockets*, Vol. 32, No. 6, pp.1033-1038.

Kluever, C. A. and Oleson, S. R. (1998). Direct Approach for Computing Near-Optimal Low-Thrust Earth-Orbit Transfers, *Journal of Spacecraft and Rockets*, Vol. 35, No. 4, pp.509-515.

Sedov, L. I. (1993). *Similarity and Dimensional Methods in Mechanics, 10th Ed.*, CRC Press, Boca Raton.

Raizer, Y. P. (1977). *Laser-Induced Discharge Phenomena*, Consultants Bureau, New York and London.

Richard, J. C., Morales, C., and Myrabo, L. N. (1988) Transatmospheric Laser Propulsion of a 100 MW-Class Lightcraft Technology Demonstrator (LTD), AIAA Paper 88-2970.

Sanders, S., et al. (1994). High Power Coherent Two-Dimensional Semiconductor Laser Array, *Applied Physics Letters*,, Vol. 64, No. 12, pp.1478-1480.

Simons, G. A. and Pirri, A. N. (1977). The Fluid Mechanics of Pulsed Laser Propulsion, *AIAA Journal*, Vol. 15, No. 6, pp. 835-842.

Shirakawa, A., Saitou, T., Sekiguchi, T., and Ueda, K. (2002). Coherent Addition of Fiber Lasers by Use of a Fiber Coupler, *Optics Express*, Vol. 10, No. 21, pp.1167-1172.

Ushio, M., Komurasaki, K., Kawamura, K., and Arakawa, Y. (2008). Effect of Laser Supported Detonation Wave Confinement on Termination Conditions, *Shock Waves*, Vol. 18, No.1, pp.35-39.

Laser Pulse Phenomena and Applications

Edited by Dr. F. J. Duarte

ISBN 978-953-307-405-4
Hard cover, 474 pages
Publisher InTech
Published online 30, November, 2010
Published in print edition November, 2010

Pulsed lasers are available in the gas, liquid, and the solid state. These lasers are also enormously versatile in their output characteristics yielding emission from very large energy pulses to very high peak-power pulses. Pulsed lasers are equally versatile in their spectral characteristics. This volume includes an impressive array of current research on pulsed laser phenomena and applications. *Laser Pulse Phenomena and Applications* covers a wide range of topics from laser powered orbital launchers, and laser rocket engines, to laser-matter interactions, detector and sensor laser technology, laser ablation, and biological applications.

How to reference

In order to correctly reference this scholarly work, feel free to copy and paste the following:

Hiroshi Katsurayma, Kimiya Komurasaki and Yoshihiro Arakawa (2010). Pulse-Laser Powered Orbital Launcher, Laser Pulse Phenomena and Applications, Dr. F. J. Duarte (Ed.), ISBN: 978-953-307-405-4, InTech, Available from: http://www.intechopen.com/books/laser-pulse-phenomena-and-applications/pulse-laser-powered-orbital-launcher

INTECH
open science | open minds

InTech Europe
University Campus STeP Ri
Slavka Krautzeka 83/A
51000 Rijeka, Croatia
Phone: +385 (51) 770 447
Fax: +385 (51) 686 166
www.intechopen.com

InTech China
Unit 405, Office Block, Hotel Equatorial Shanghai
No.65, Yan An Road (West), Shanghai, 200040, China
中国上海市延安西路65号上海国际贵都大饭店办公楼405单元
Phone: +86-21-62489820
Fax: +86-21-62489821